Titanium-Niobium (Ti-xNb) Alloys with High Nb Amounts for Applications in Biomaterials

Bruno Leandro Pereira[a,c]* (ID)*, Carlos Maurício Lepienski[a,b,d], Viviane Seba[c], Guibert Hobold[e],*

Paulo Soares[d,g] (ID)*, Bor Shin Chee[c], Pedro Akira Bazaglia Kuroda[f] ,Erico Saito Szameitat[a],*

Leonardo Luís dos Santos[a], Carlos Roberto Grandini[f] (ID)*, Michael Nugent[c]*

[a]Universidade Federal do Paraná, Programa de Pós-Graduação em Engenharia e Ciência dos Materiais (PIPE), Curitiba, PR, Brasil.
[b]Universidade Federal do Paraná, Departamento de Física, 81531-980, Curitiba, PR, Brasil.
[c]Athlone Institute of Technology, Athlone, Ireland.
[d]Universidade Tecnológica Federal do Paraná, Departamento de Engenharia Mecânica, 81531-980, Curitiba, PR, Brasil.
[e]Pontifícia Universidade Católica do Paraná, Departamento de Engenharia Mecânica, 80215-901, Curitiba, PR, Brasil.
[f]Universidade Estadual Paulista (UNESP), Laboratório de Anelasticidade e Biomateriais, Bauru, SP, Brasil.
[g]Colorado State University, Department of Mechanical Engineering, United States of America.

The present study produced binary titanium-niobium alloys Ti-xNb with high niobium percentage (x = 50, 80 e 90 wt.%) aiming to apply it as a base material in osseous implant devices. The produced TiNb alloys presented a cubic crystalline phase, lower corrosion rate than titanium, lower elastic modulus values, and superior cellular viability than titanium and niobium. The Ti50Nb alloy among all analyzed metallic substrates showed the best values of elastic modulus, corrosion properties, wettability, and cellular viability. Thus, this work suggests a Ti/Nb ratio close to 1 (Ti50Nb) displays optimum characteristics to apply in orthopedic devices.

Keywords: Niobium, Titanium, elastic modulus, TiNb alloys, corrosion resistance.

1. Introduction

Metallic materials have been widely used as orthopedic and dental implants for decades, as they generally have more suitable mechanical properties to resist medium and long periods of usage[1]. However, the human body is a chemically aggressive environment and sensitive to the toxicity of most metal ions[2-4]. Thus, the variety of metals that can be used as implants is very restricted. Further, another problem to be solved is the lack of adequate mechanical stimulation around the implanted material, which can result in local bone loss[5]. To avoid compromising the mechanical stability caused by loss of bone mass, the material used must have elastic modulus (E) closer to the value of bone tissue (< 40 GPa)[3].

Commercially pure titanium cp-Ti is a low density, biocompatible, and corrosion-resistant metal; however, its mechanical properties limit its application[6,7]. Typically, cp-Ti is used for non-load-bearing usages such as dental, maxillofacial, and craniofacial implants, screws, and staples for surgeries[8]. Pure Nb is biocompatible, has excellent corrosion resistance, and elastic modulus considerably lower than Ti[4,6]. However, Nb is not used as implants, but as a substitutional element in Ti alloys.

Ti alloys can be classified according to their microstructure as α, super α, α-β, and β[4]. The α and super α alloys do not present significant advantages over Ti-cp. α-β alloys, such as Ti-6Al-4V, have better mechanical properties (fatigue and ultimate tensile strength) compared to Ti-cp and can be used in load-bearing applications such as femoral stem prosthesis[2]. However, the α-β alloys have poor bending ductility, which can cause a premature failure at the neck of the femoral stem, and the use of vanadium (V) and aluminum (Al) has been questioned due to its possible toxicity[2]. β -Ti alloys have advantages such as low elastic modulus, good corrosion resistance, better bending ductility, and biocompatibility compared to Ti-6Al-4V and other α - β alloys. The β alloys are designed to be free of vanadium V, composed of non-toxic elements like Nb and tantalum Ta[2,4]. In β Ti alloys, Nb acts as a strong β stabilizer. Ti alloys can become completely β at room temperature by adding a percentage above 25% atomic (40% wt.) of Nb[9].

Binary Ti-xNb alloys (x% wt.) are being studied for application in biomaterials. Ti-xNb alloys (x = 5-25%, and 45% wt.) presented better mechanical properties and similar biocompatibility compared to Ti-cp[10,11]. Ti-xNb alloys (x = 45 and 50% wt.) showed higher hardness and considerably lower elastic modulus than Ti-cp and Ti-6Al-4V[12]. It has been shown that the ultimate tensile strength, hardness, yield strength, hydrophilicity, corrosion resistance increase with increasing Nb percentage[10,13,14].

Despite the mechanical and biological characteristics showing improvement with increasing the amount of Nb in Ti-xNb binary alloy, there are practically no studies with percentages higher than 50% wt. of Nb. The main reasons, according to the literature, are that Nb is a rare metal with a high melting point, which would make the alloy production process expensive[10,15,16]. However, Nb production is high due to Brazilian deposits that extract more than 90% of Nb's total world production. Brazil produced 8×10^4 Ton/year (2015-2018) of Nb, and in 2019 the production reached 11×10^4 Ton[17]. Comparatively, the world production of vanadium V was 7.3×10^4 Ton in 2019[18]. That is, currently, Nb is not a rare metal. Thus, the present study aimed to produce Ti-xNb alloys with high Nb percentages (x=50, 80, 90% wt.) and to evaluate the mechanical properties, corrosion resistance, and cell viability for application in biomedical implants.

2. Materials and Methods

2.1 Production of Ti-xNb alloys (x = 50%, 80%, and 90% wt.)

The materials used to produce the alloys were commercially pure titanium grade 2, with 99.7% purity, and niobium with 99.8% purity. The metal masses were measured by an analytical scale to obtain the alloys with 50%, 80%, and 90% weight of Nb. Ti-Nb alloys were melted in an arc-furnace, with a water-cooled copper crucible, non-consumable tungsten electrode, and a controlled argon atmosphere. The raw materials, Ti and Nb, were melted 5 times to ensure good homogeneity. The melting procedure was carried out in a vacuum of 10^{-2} mBar to remove impurities from the atmosphere. After melting, a homogenization heat treatment was carried out to relieve the residual internal stresses from the fusion. The alloys were heat-treated in an ultra-high vacuum for 24 hours at 1000°C.

2.2 Surface preparation

The Ti-xNb ingots (x = 50%, 80% and 90%) were cut by Wire EDM (electrical discharge machining), followed by polishing sequentially with 220, 320, 360, 600, 1000, 1200, and 2000 (grit size) sandpaper. The metals and binary alloys were then polished with colloidal silica solution diluted in hydrogen peroxide (15% vol. H_2O_2). cp-Ti and pure Nb plates were also used to compare the Ti-xNb alloy's performance and were prepared using the same surface preparation procedure applied to the alloys. The alloys were named Nb50 (Ti50Nb), Nb80 (Ti80Nb), and Nb90 (Ti90Nb).

All specimens were cleaned in propanone, ethanol, and distilled water, for 15 min in each solvent in an ultrasonic bath. Then, the specimens were inserted in a dryer for 24 h at a constant temperature of 40 °C.

2.3 Samples characterization

Samples were analyzed by scanning electron microscopy (Vega3, Tescan) using a magnification of 1 kX. The chemical compositions were evaluated by energy-dispersive X-ray spectroscopy (x-act, Oxford) applying energy of 15 keV. For each alloy surface, a map with a chemical composition was generated.

The alloy crystalline phases were identified by the X-ray diffraction technique XRD applying the Bragg-Brentano geometry. The tests were performed in the $15° \leq \theta \leq 90°$ angle range with Cu-Kα radiation. The XRD equipment used was a Shimadzu-XRD7000 with a monochromator coupled.

To reveal the Ti-xNb alloys' microstructures, the alloy surfaces were etched with an acid solution composed of HF, HCl, HNO_3, and distilled water (following the proportions of the reference[14]). After that, the microstructure images were obtained by optical microscopy. The grain boundaries were highlighted by image software.

The mechanical properties were measured using a nanoindenter ZHN (Zwick-Roell). It was made 49 indentations per specimen with a Berkovich tip. The tests were performed using the QCSM (*Quasi Continuous Stiffness Measurement*) and the maximum force for all indentations was 500 mN.

The wettability measurements were made using a goniometer (FTA 1000 Analyzer System, First Ten Angstroms Inc., USA). For each measurement, the water drop of 1 µl remained lied on the surface for 40 s and, after that, the angle between the water drop and the metallic surfaces was collected and measured by the equipment.

The surface roughness of the specimens was measured using an Olympus confocal laser microscope LEXT OLS 4000. The OLS 4000 software was used to obtain images and, consequently, the parameters of roughness. Roughness parameters 3D and 2D (dimensions) of each specimen were designated by the letters S and R, respectively. The size of the evaluated areas was 258 x 258 µm².

The experimental corrosion setup was composed of an Ivium Technologies potentiostat, three electrodes (platinum electrode, the metallic specimen, and a saturated calomel electrode) soaked in 150 ml of PBS (phosphate buffer solution) contained in an acrylic electrolytic cell. The corrosion test was carried out through the potentiodynamic polarization technique applying a potential difference range of -1.5 V to 2.5 V for 1 hour at 25^0 C.

The viability of the MC3T3 osteoblast cell lines was analyzed by MTT assay. The MC3T3 cells were cultured in Alpha minimum essential medium, supplemented with 10% FBS, 100 U/ml penicillin, and 100 µg/ml streptomycin. The cells were cultured at 37°C in a humidified atmosphere of 5% CO_2.

The titanium was placed in 24-well culture plates and the osteoblast cells were seeded at a concentration of 50.000 cells/well in three replicates and incubated for 48h. After this period, the medium was replaced with fresh medium and 50 µL of a solution of MTT (3-(4,5-dimethylthiazol-2-yl)-2,5-diphenyltetrazolium bromide) (Sigma-Aldrich®) (5 mg/mL) was added to each well, and the plates were incubated for 3 h at 37 °C. Next, 200 µL (each well) of the medium with MTT was removed from the 24-well plates and replaced with 96-well plates, and finally, cell viability was quantified by the detection of absorbance (550 nm) in a microplate reader (BioTek Synergy HT).

3. Results

Table 1 displays the percentage of the alloy by atomic weight also obtained from the EDS technique. In this analysis, the natural layer's oxygen element covering the alloys and the

Table 1. Percentage by weight of the chemical elements obtained by EDS, density, and roughness of alloys and polished metals.

Specimen	Nb (%)	Ti (%)	Theoretical density (g.cm^{-3})	Measured density (g.cm^{-3})	Roughness Sa (µm)	Roughness Ra (µm)
Nb50	49.5 ± 0.3	50.5 ± 0.3	6.507	6.5 ± 0.6	0.030 ± 0.005	0.014 ±0.002
Nb80	80.9 ± 0.2	19.1 ± 0.2	7.707	7.8 ± 0.4	0.06 ± 0.01	0.005 ± 0.01
Nb90	89.8 ± 0.2	10.4 ± 0.2	8.107	8.2 ± 0.4	0.041 ± 0.007	0.03 ± 0.01
Nb	100	0	8.570		0.018 ± 0.008	0.008 ± 0.0005
Ti	0	100	4.507		0.05 ± 0.01	0.02 ± 0.01
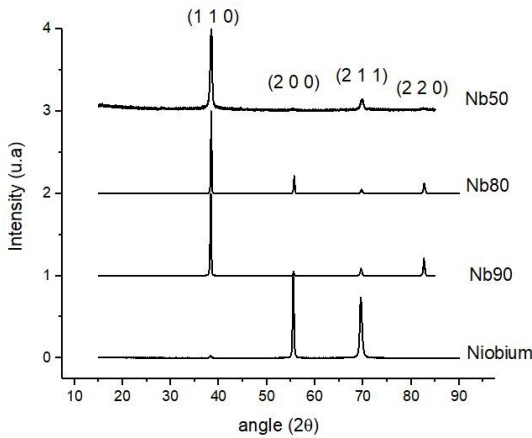
Figure 1. X-ray diffraction spectra of the polished specimens of niobium, Nb50, Nb80, and Nb90 alloys.

silicon remnants from the polishing process were subtracted from the average. The polishing process was carried out until the surfaces was mirrored, which produced surfaces with very low roughness - nanometric range.

Figure 1 shows the diffractogram of the Nb and the alloys related to this study. All alloys presented only the β phase. The peaks in the spectrum are related to niobium (body-centered cubic) and β-Ti.

The microstructure of the alloys were observed by optical microscopy (Figure 2) after successive polishing and acid etching with the Kroll solution. All alloys presented grains boundary with equiaxial characteristics. The Nb50 alloy has larger grains, while there are no significant differences between the Nb80 and Nb90 alloys.

The polished and cleaned specimens were subjected to mechanical tests through the nanoindentation technique. Figure 3 shows the elastic modulus (E) and the hardness (H) of the studied substrates for a depth of 3 µm. Comparatively, the samples of pure niobium Nb and the alloys with 80 and 90% niobium did not present significant differences regarding E and H. The Nb, Nb90, Nb80, and Nb50 displayed elastic modulus equal to 99 GPa, 98 GPa, 97 GPa, 79 GPa, and hardness equal to 1.9 GPa, 1.8 GPa, 1.9 GPa, and 2.16 GPa, respectively, at the measured depth of 3 µm. When compared to commercially pure Ti grade 2, the elastic modulus of Nb and alloys showed considerably lower values of E.

Table 2 shows the electrochemical parameters of the Ti, Nb, and alloys obtained by analyzing the potentiodynamic polarization curves alloys from Figure 4. The electrical potential of corrosion showed to be nobler (greater),

increasing the niobium percentage. As for the corrosion current i_{cor} (and consequently, the current density J_{cor}) it increases with increasing the amount of niobium. However, the Nb90 showed a higher i_{cor} than the Nb. Titanium, on the other hand, presented the highest corrosion current among all analyzed substrates.

As for the polarization resistance, Nb90 presented the lowest value among all substrates, Ti showed the highest value among metals, and Nb80 displayed the highest value among all analyzed substrates. Polarization resistance R_p is inversely proportional to i_{cor}. However, the values also are dependent on the b_a and b_c constants[19], as shown in Equation 1.

$$i_{cor} = \frac{b_a \cdot b_c}{2.303(b_a + b_c)} \frac{1}{R_p} \qquad (1)$$

To calculate the corrosion rate C_R, the specific mass ρ, current density J_{cor}, and the equivalent weight (EW) were used (to calculate EW see the references[19,20]). These values were applied to Equation 2 to find the C_R.

$$C_R = K \frac{J_{cor} \cdot EW}{\rho} \qquad (2)$$

Where the constant K = 3.27 mm·g· A^{-1}·cm^{-1}·yr^{-1}.

The Nb50 alloy showed the lowest corrosion rate, followed by Nb80. The Nb presented the best value among the metals, while the Ti presented the highest corrosion rate per year among all analyzed materials.

Figure 4 shows the potentiodynamic polarization curves of Ti-xNb, niobium, and titanium alloys in PBS (Phosphate-buffered saline) solution. In this experiment, the electrical potential difference between the sample and the reference electrode varied from -1.5 V to 2.5 V. As an answer to the electrical potential difference, a current of electric charge carriers (ions and electrons) passes through the experimental system and it is measured and presented on a logarithmic scale.

All curves presented corrosive characteristics with similar curves. The region between the horizontal dashed lines shows a "bending" (-0.06 V to 0.08 V) in the curves that indicate the passive layer formation on the metallic substrate. After "bending" in the curves, a plateau appears (little variation in current density) characteristic after the formation of the protective oxide layer. This layer hinders the passage of current and when it is damaged, a sudden increase in current is observed. In Figure 4 it is indicated by arrows and by values of the corresponding electrical potentials that have broken the passive film. Among the specimens, the alloys Nb80 and Nb50 did not show signs of rupture of the protective film at the analyzed electric potential range. However, the Nb90, Nb, and Ti presented for 1.18 V, 1.61 V,
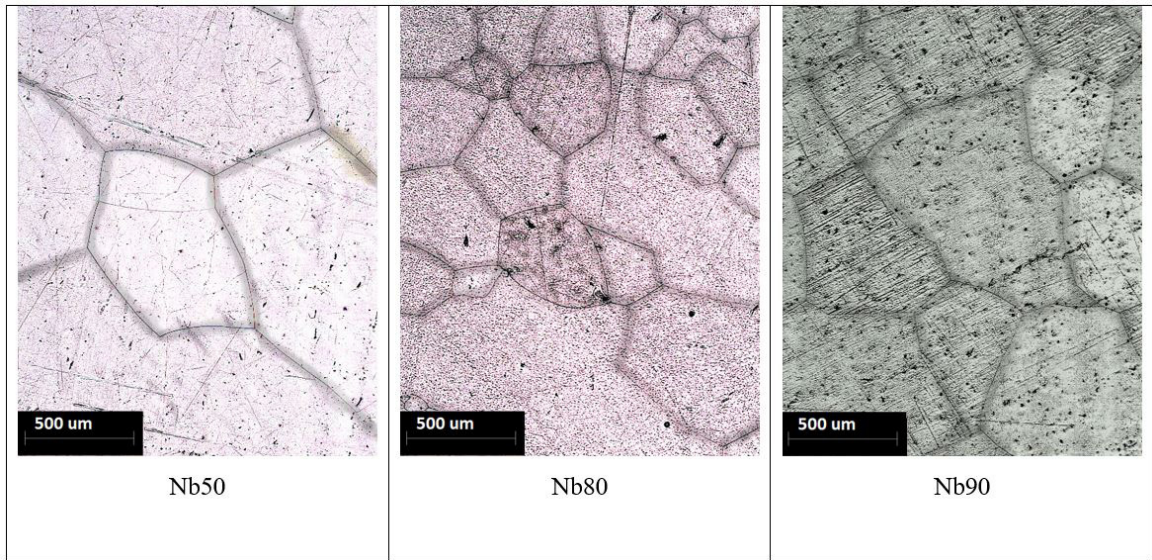
Figure 2. The microstructure of the polished alloys (Nb50, Nb80, and Nb90) and subsequently acid-etched with Kroll solution. The images were obtained by optical microscopy with the grain boundaries lines highlighted by image software.
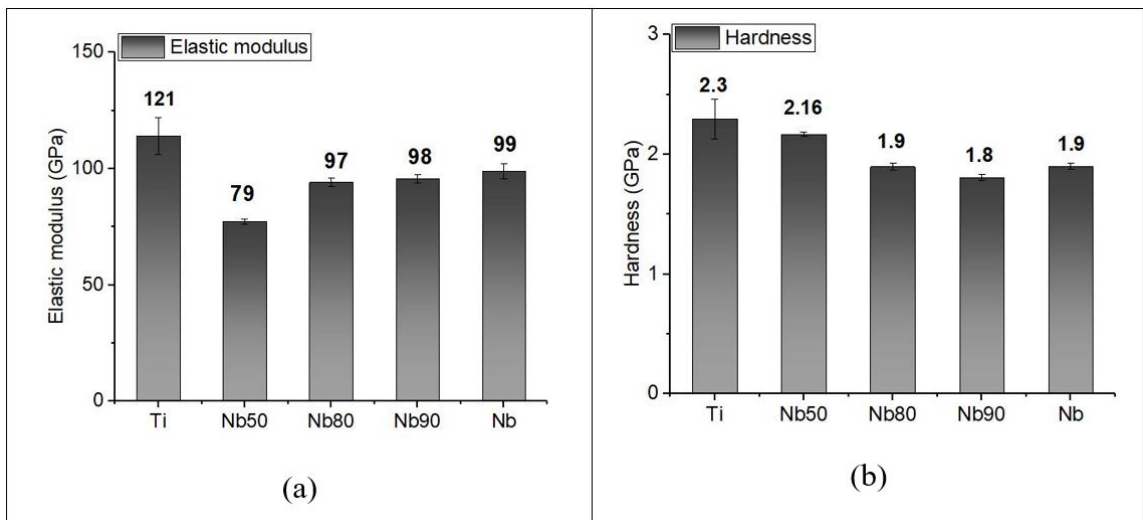

Figure 3. Elastic moduli (a) and hardness (b) of polished samples of Nb, Ti and Nb50, Nb80, and Nb90 alloys at an approximate penetration depth of 3μm.

Table 2. Electrochemical parameters obtained by the polarization curves in Figure 4.

Electrochemical parameters	Ti	Nb50	Nb80	Nb90	Nb
E_{cor} (V)	-0.6125	-0.5965	-0.5715	-0.4984	-0.4585
i_{cor} (10^{-5} A)	5.59	2.00	2.19	4.97	3.38
J_{cor} (10^{-5} A.cm^{-2})	4.94	1.77	1.94	4.39	2.99
Polarization resistance (10^9 Ω)	1.53	1.46	1.64	0.869	1.20
b_a (V/decade)	0.744	0.163	0.283	0.210	0.218
b_c (V/decade)	0.266	0.114	0.117	0.189	0.164
Equivalent weight EW	11.98	14.56	16.73	17.61	18.58
Corrosion rate (10^{-2} mm/ano)	4.30	1.30	1.37	3.12	2.12

and 1.91 V, respectively. Another observable point is that less current flows through the alloys Nb80 and Nb50 (their plateaus are localized more to the left side).

The polished surfaces of Nb, Ti, and the alloys were subjected to tests of wettability, cell viability with MTT as shown in Figure 5. The smallest angle found (more hydrophilic surface) was for the Nb50 alloy, followed by Nb80, Ti, Nb90, and Nb. For the cell adhesion test, the test performance was normalized from Ti (Ti = 100%), as it is the most studied by the scientific community among the substrates in this work.

The 50Nb alloy presented an average performance of 25% higher than Ti. Nb80 and Nb90 showed an improvement of 16% and 4%, respectively. At the same time, Nb performed slightly below (-3%). The number of cells attached presented a direct relation to the surface hydrophilicity. Regarding roughness, no relation was detected between surface roughness and density of adhered cells or wettability.
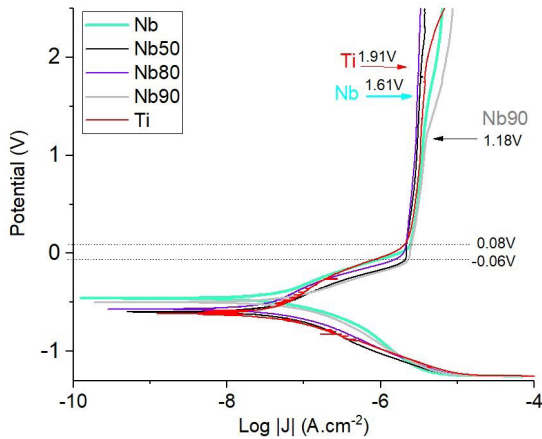

Figure 4. Potentiodynamic polarization curves of Nb 90, Nb 80, Nb50, titanium, and niobium.

4. Discussion

The process of alloys production was carried out successfully, as the component elements are well distributed following the proportions previously projected, and the specific mass of the alloys are close to the calculated theoretical values.

X-ray diffraction showed only the presence of peaks referring to niobium and the β phase of Ti, compared with the patterns #34-370 (Nb) and #44-1288 (β-Ti) of the database PDF2. It is noteworthy that the position, concerning the x-axis, the peaks of Nb and β-Ti do overlap, that is, it is not possible to distinguish them in this way. In this study, several X-ray diffraction measurements were performed, where three specimens of each alloy/metal were used, which were also rotated in 180 degrees. It was observed that the diffraction patterns almost not changed. The revealed grains of the alloys Nb90, Nb80, and Nb50 are of the equiaxial type, which is a typical feature of the complete formation of the beta phase[14], which is according to the XRD spectra.

For application in biomaterials, the material which will be in contact with bone tissue should have an elastic modulus E closer to the E of the bone tissue (<40GPa) to avoid the stress shielding effect and high hardness to guarantee its integrity after mechanical stresses[2]. In this regard, the substrate that comes closest to the desired mechanical qualities was the Nb50. The Nb50 showed an elastic modulus of 79 GPa and hardness of 2.16 GPa. The Nb80 (97GPa) and Nb90 (98GPa) alloys showed E values slightly lower than the Nb (99GPa). The values of E for Nb and alloys are considerably lower than the E of the Ti (114GPa) and α + β Ti alloys (~120GPa), which are widely used as materials in implants[16].

The range of electric potential difference E_p concerning the reference electrode was sufficient because the characteristic curves were formed. Besides, the human body does not typically exceed the E_p of 2.5 V[20], which is following the purpose of this study. Regarding the performance of substrates, materials with a corrosion rate lower than 0.1 mm per year are considered resistant to corrosion and can be used without restriction[21]. That is, in the PBS solution at room
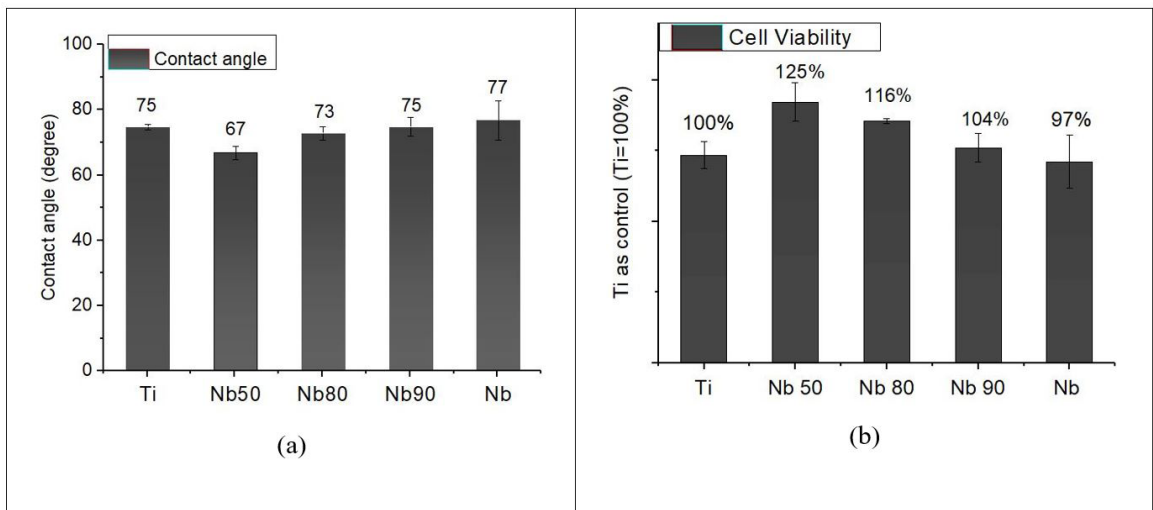

Figure 5. Contact angle of the water drops deposited on the specimens (a) and their respective cell viability (b).

temperature, all substrates demonstrated excellent corrosion resistance, and the Nb80 and Nb50 alloys presented the lowest corrosion rates.

With the increase in electrical potential concerning the reference electrode, the anodizing process begins, increasing the protective oxide layer. The most efficient layers are those that show no signs of breaking and allow less current to flow through. The Nb80 alloy followed by the Nb50 showed the most efficient protective oxide layers as they did not show signs of breaking (current increase) and lower current flow among all analyzed substrates.

The corrosion potential increases with the amount of Nb in the analyzed substrates, which can be seen by the lateral peaks in Figure 4 and Table 2. It was also observed for Kaseen and Choe for alloys with lower amounts of Nb. In that same study, it was evaluated that the corrosion rate of the Ti-xNb alloys (x= 10%, 30%, and 50% wt.) improve with the increasing percentage of Nb[14]. In the case of our study, the corrosion rate improves (decreases) with the decrease of the Nb percentage. That is, there is a tendency for ratios of Ti / Nb (weight) close to 1 to show better anti-corrosion performances in the conditions of this experiment.

As for the wettability test, there were no significant differences in the measured contact angles with water on all surfaces, and all surfaces may be classified as hydrophilic (contact angle $< 90^0$)[22]. In Ti-xNb alloys (5, 10, 20, 25), Zhang noted that the greater the amount of Nb, the more hydrophilic was the surface[10]. However, we found an inverse relation, the less Nb in the alloys the more hydrophilic the surface. It suggests that Ti-xNb alloys with a Ti / Nb (wt.) ratio close to 1 tend to present more hydrophilic surfaces.

The surface hydrophilicity is considered one of the main factors that improve cell adhesion[23,24]. Even though there were no significant differences of hydrophilicity on the alloys, Nb, and Ti, it caused variations in the number of bone cells per unit area adhered to the surfaces. Summing up, increasing the surface hydrophilicity there were improvements in the cell viability. Among all substrates, the Nb50 and Nb80 presented cell-test performance 25% and 16% superior to the Ti, respectively.

Besides the wettability, roughness can also influence cell adhesion[24]. The specimens were polished up to mirroring and presented nanometric roughness. The surfaces displayed variations on the roughness. However, any influence was detected on cell-test performance.

5. Conclusion

Titanium-Niobium binary alloys were produced in the Nb proportions of 50% (Nb50), 80% (Nb80), and 90% (Nb90) by weight for application in the field of orthopedic and orthodontic implants. The binary alloys were compared with the pure metals of the alloy (Nb and Ti) and the results were:

• XRD spectra showed only the cubic crystalline phase formation for all alloys.
• All alloys and Nb presented better values of elastic modulus for use in implants when compared to Ti. Among the Ti alloys, the Nb50 demonstrated the best value of elastic modulus and the highest hardness.
• All alloys and Nb showed lower corrosion rates than Ti in PBS solution. The Nb50 and Nb80 alloys

showed the lowest corrosion rates and more efficient protective oxide layers.
• The number of cells attached presented a direct relation to the surface hydrophilicity. Regarding roughness, no relation was detected between surface roughness and density of adhered cells or wettability.

Comparing the results of this work with studies of binary alloys with lower percentages of Nb (Nb < 50%) in literature, it is possible to conclude that ratios by weight of Ti/Nb ~ 1 tend to present optimal characteristics for application in osseous implants.

6. Acknowledgments

7. References

1. Davis JR. Handbook of materials for medical devices. Materials Park: ASM International; 2003 [cited 2020 Sep 5]. Available from: http://books.google.com.br/books?id=JEJRAAAAMAAJ
2. Chen Q, Thouas GA. Metallic implant biomaterials. Mater Sci Eng Rep. 2015;87:1-57. http://dx.doi.org/10.1016/j.mser.2014.10.001.
3. Musa A. Overview of biomaterials and their use in medical devices. In: Davis JR, editor. Handbook of materials for medical devices. Materials Park: ASM International; 2003. http://dx.doi.org/10.1361/hmmd2003p001.
4. Niinomi M. Recent metallic materials for biomedical applications. Metall Mater Trans, A Phys Metall Mater Sci. 2002;33(3):477-86. http://dx.doi.org/10.1007/s11661-002-0109-2.
5. Ridzwan MIZ, Shuib S, Hassan AY, Shokri AA, Ibrahim MNM. Problem of stress shielding and improvement to the hip implant designs: a review. J Med Sci. 2007;7(3):460-7. http://dx.doi.org/10.3923/jms.2007.460.467.
6. Matsuno H, Yokoyama A, Watari F, Uo M, Kawasaki T. Biocompatibility and osteogenesis of refractory metal implants, titanium, hafnium, niobium, tantalum and rhenium. Biomaterials. 2001;22(11):1253-62. http://dx.doi.org/10.1016/S0142-9612(00)00275-1. PMid:11336297.
7. Geetha M, Singh K, Asokamani R, Gogia K. Ti based biomaterials, the ultimate choice for orthopaedic implants: a review. Prog Mater Sci. 2009;54(3):397-425. http://dx.doi.org/10.1016/j.pmatsci.2008.06.004.
8. Lütjering G, Williams JC. Titanium. Berlin: Springer; 2007 [cited 2020 Sep 5]. Available from: https://books.google.com.br/books?id=c9iR1Lm43GEC
9. Gutiérrez Moreno JJ, Bönisch M, Panagiotopoulos NT, Calin M, Papageorgiou DG, Gebert A, et al. Ab-initio and experimental study of phase stability of Ti-Nb alloys. J Alloys Compd. 2017;696:481-9. http://dx.doi.org/10.1016/j.jallcom.2016.11.231.
10. Zhang Y, Sun D, Cheng J, Tsoi JKH, Chen J. Mechanical and biological properties of Ti-(0-25 wt%)Nb alloys for biomedical implants application. Regen Biomater. 2020;7(1):119-27. http://dx.doi.org/10.1093/rb/rbz042. PMid:32153995.
11. Bai Y, Deng Y, Zheng Y, Li Y, Zhang R, Lv Y, et al. Characterization, corrosion behavior, cellular response and in vivo bone tissue

compatibility of titanium-niobium alloy with low Young's modulus. Mater Sci Eng C Mater Biol Appl. 2016;59:565-76. http://dx.doi.org/10.1016/j.msec.2015.10.062. PMid:26652409.

12. Martins GV, Silva CRM, Nunes CA, Trava-Airoldi VJ, Borges LA, Machado JPB. Beta Ti-45Nb and Ti-50Nb alloys produced by powder metallurgy for aerospace application. Mater Sci Forum. 2010;660-661:405-9. http://dx.doi.org/10.4028/www.scientific.net/MSF.660-661.405.

13. Silva LM, Claro APRA, Buzalaf MAR, Grandini CR. Influence of the substitutional solute on the mechanical properties of Ti-Nb binary alloys for biomedical use. Mater Res. 2012;15(3):355-8. http://dx.doi.org/10.1590/S1516-14392012005000040.

14. Kaseem M, Choe HC. Electrochemical and bioactive characteristics of the porous surface formed on Ti-xNb alloys via plasma electrolytic oxidation. Surf Coat Tech. 2019;378:125027. http://dx.doi.org/10.1016/j.surfcoat.2019.125027.

15. Bönisch M, Calin M, Van Humbeeck J, Skrotzki W, Eckert J. Factors influencing the elastic moduli, reversible strains and hysteresis loops in martensitic Ti-Nb alloys. Mater Sci Eng C Mater Biol Appl. 2015;48:511-20. http://dx.doi.org/10.1016/j.msec.2014.12.048. PMid:25579952.

16. Abdel-Hady Gepreel M, Niinomi M. Biocompatibility of Ti-alloys for long-term implantation. J Mech Behav Biomed Mater. 2013;20:407-15. http://dx.doi.org/10.1016/j.jmbbm.2012.11.014. PMid:23507261.

17. Bica VHF, Nemoto YL. Anuário Mineral Brasileiro: principais substâncias metálicas-2019. Brasília: Agência Nacional de Mineração– ANM. (2019) 1–112. Available from: http://antigo.anm.gov.br/portal/dnpm/publicacoes/serie-estatisticas-e-economia-mineral/anuario-mineral/anuario-mineral-brasileiro/amb_2019_ano_base_2018/@@download/file/AMB_Metalicos_2019.pdf.

18. USGS: United States Geological Survey. Mineral Commodity Summaries 2020. Reston; 2020. [cited 2020 Sep 5]. Available from: https://www.usgs.gov/centers/nmic/mineral-commodity-summaries

19. ASTM: American Society for Testing and Materials. ASTM G102-89(2015): standard practice for calculation of corrosion rates and related information from electrochemical measurements. West Conshohocken: ASTM International; 2015.

20. Burnat B, Walkowiak-Przybyło M, Błaszczyk T, Klimek L. Corrosion behaviour of polished and sandblasted titanium alloys in PBS solution. Acta Bioeng Biomech. 2013;15(1):87-95. http://dx.doi.org/10.5277/abb130111. PMid:23957237.

21. Ponte H. A. Fundamentos da corrosão. Curitiba: Universidade Federal do Paraná; 2003.

22. Kanduč M, Schneck E, Netz RR. Attraction between hydrated hydrophilic surfaces. Chem Phys Lett. 2014;610–611:375-80. http://dx.doi.org/10.1016/j.cplett.2014.07.046.

23. Arima Y, Iwata H. Effect of wettability and surface functional groups on protein adsorption and cell adhesion using well-defined mixed self-assembled monolayers. Biomaterials. 2007;28(20):3074-82. http://dx.doi.org/10.1016/j.biomaterials.2007.03.013. PMid:17428532.

24. Anselme K. Osteoblast adhesion on biomaterials. Biomaterials. 2000;21(7):667-81. http://dx.doi.org/10.1016/S0142-9612(99)00242-2. PMid:10711964.